Chapter 9
Special Plasmas

9.1 Non-Neutral Plasmas

9.1.1 Pure Electron Plasmas

The concepts of plasma physics have so far been couched in terms of well-behaved, quasineutral plasmas, but there are other plasmas with special properties. Particle accelerators have a single species, but the kinematic effects are so large that the collective effects are not important. It is possible to generate single-species plasmas at low densities such that the electric fields are manageable. Ronald Davidson, Malmberg and O'Neil, Dan Dubin, and others have developed this interesting topic. Consider an infinite cylinder of electrons of uniform density n_0 in a uniform coaxial magnetic field $\mathbf{B}$ (Fig. 9.1). A large electric field $\mathbf{E} = E_r(r)\hat{\mathbf{r}}$ will arise, (where E_r is negative), and a typical fluid element of electrons will drift in a circular orbit, since everything is azimuthally symmetric. Those with small, off-axis orbits will drift around the axis in "diocotron" orbits, as shown at the right. We wish to calculate the rotation frequency ω_r:

$$\omega_r(r) \equiv v_\theta(r)/r. \tag{9.1}$$

In equilibrium, the inward and outward forces will balance:

$$\begin{aligned} mv_\theta^2(r)/r &= -eE_r(r) - ev_\theta(r)B \\ mr\omega_r^2 &= -eE_r - ev_\theta B = -eBr\omega_r - eE_r \end{aligned} \tag{9.2}$$

The radial E-field is found from Poisson's equation:

F.F. Chen, *Introduction to Plasma Physics and Controlled Fusion*,
DOI 10.1007/978-3-319-22309-4_9

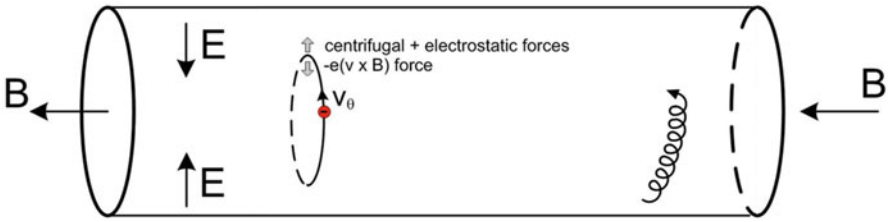

Fig. 9.1 A non-neutral plasma of electrons. (Adapted from R.C. Davidson, *Physics of Nonneutral plasmas* (Addison-Wesley, Redwood City, CA, 1990)).

$$\begin{aligned}\frac{1}{r}\frac{d}{dr}(rE_r) &= -en_e/\varepsilon_0 \\ rE_r &= \frac{-en_e}{\varepsilon_0}\int_0^r r'dr' = \frac{-en_e r^2}{2\varepsilon_0} \\ E_r &= -\frac{r}{2}\frac{en_e}{\varepsilon_0} = -\frac{r}{2}\frac{m}{e}\omega_p^2 \qquad r \le a\end{aligned} \tag{9.3}$$

Equation (9.2) then becomes

$$\begin{aligned}\omega_r^2 + \omega_c\omega_r + \frac{eE_r}{mr} &= \omega_r^2 + \omega_c\omega_r - \tfrac{1}{2}\omega_p^2 = 0 \\ \omega_r &= \tfrac{1}{2}\omega_c\left[-1 \pm \left(1 - 2\omega_p^2/\omega_c^2\right)^{1/2}\right].\end{aligned} \tag{9.4}$$

Since ω_r is independent of radius, we see that such an pure electron plasma rotates as a solid body. When $\omega_p^2/\omega_c^2 > \tfrac{1}{2}$, there is no solution; otherwise, there are two solutions. For $2\omega_p^2/\omega_c^2 << 1$, expanding the square root yields the frequencies $\omega_r \approx -\omega_c$, and the lower frequency

$$\omega_r \approx \omega_p^2/2\omega_c \equiv \omega_D. \tag{9.5}$$

Called the *diocotron* frequency, ω_D has an orbit like the one at the right in Fig. 9.1.

With appropriate modifications, these equations can also describe pure ion plasmas. Both types of single-species plasmas have been produced and studied in the laboratory.

9.1.2 Experiments

A device called a Malmberg-Penning trap, shown in Fig. 9.2, is commonly used to study single-species plasmas. This useful device evolved from the work of

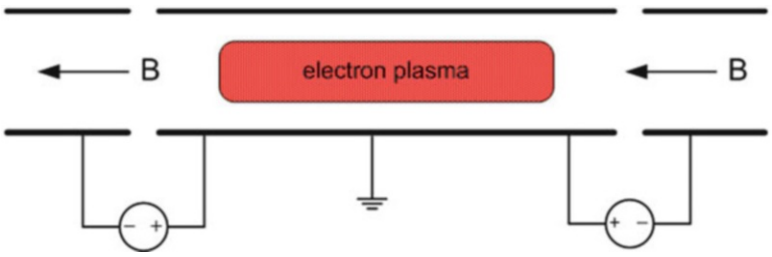

Fig. 9.2 A Malmberg-Penning trap for electrons

Wolfgang Paul, Hans Dehmelt, and Norman Ramsey,[1] who won the Nobel Prize in 1989. The trap consists of three coaxial, conducting cylinders, with the ends biased negatively to trap electrons and positively to trap ions. Conservation of canonical angular momentum can be used to show that the particles are trapped unless they make a collision with a stray neutral atom or with a error field due to imperfect machining of the container. The physical reason for this can be seen from Fig. 5.16, which shows that like-particle collisions do not cause diffusion.

As an example of what can be done with these plasmas, F. Anderegg et al. studied diffusion due to long-range interactions. Recall that Spitzer diffusion (Eq. (5.71)) had an arbitrary cutoff related to the Debye length. Ion-ion diffusion was quantified in an ion trap with LIF (laser-induced fluorescence) diagnostics. In the data shown in Fig. 9.3, one sees that the measured diffusion coefficient is an order of magnitude larger than "classical" but is closer when collisions in large-orbit $\mathbf{E} \times \mathbf{B}$ drifts are included.

9.2 Solid, Ultra-Cold Plasmas

By freezing the plasma in an ion trap to sub-Kelvin temperatures, it is possible to create liquid and solid plasmas. As the thermal motions of the particles decrease, their thermal energies become comparable to the Coulomb energy W_c between particles. This condition can be quantified by defining a coupling parameter Γ, the ratio between the average W_c and KT. Two singly charged particles separated by a distance a have a Coulomb energy e^2/a. Hence

$$\Gamma = e^2/aKT. \tag{9.6}$$

[1] The author's thesis adviser.

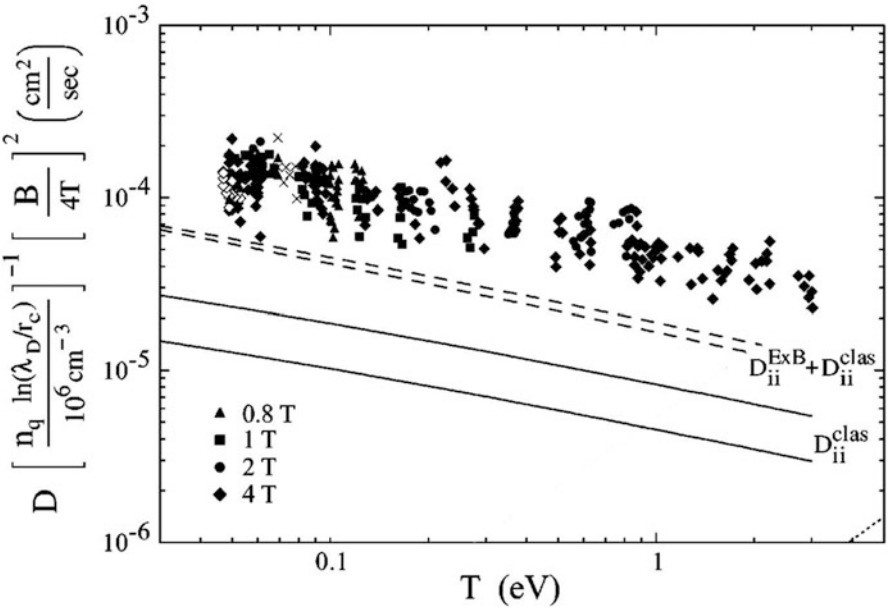

Fig. 9.3 Ion-ion diffusion coefficient compared with theory. The double lines show the expected range. (Adapted from F. Anderegg et al., Phys. Rev. Lett. **78**, 2128 (1997))

The average interparticle distance a should vary as $n^{1/3}$, but the coefficient depends on the shape of the enclosing volume. The value of a can be approximated by the Wigner-Seitz radius:

$$a = (3/4\pi n)^{1/3} \approx 0.62 n^{1/3}. \tag{9.7}$$

When Γ, as defined by Eqs. (9.6) and (9.7), becomes large, the plasma first turns into a liquid as fluid elements become highly correlated. At $\Gamma > 174$, the plasma becomes a solid crystal such as the one shown in Fig. 9.4. To achieve such a large value of Γ, the plasma is cooled to a temperature of 10 mK (10 milliKelviin, or 0.01 K) by laser cooling. In this process, a laser is tuned to a frequency just below that of a transition in the atom. A laser photon is absorbed only by atoms moving rapidly toward the laser with a blue Doppler shift. The atom's momentum is lowered by that of the photon. The photon is later re-emitted in a random direction at a lower frequency, so that the fastest atoms are removed, and the plasma is cooled.

The Penning trap is a useful device in which unusual plasmas have been created. For instance, a positronium plasma has been formed, consisting of positrons and electrons, with no ions. Also possible is the creation of anti-hydrogen, whose atoms consist of negative antiprotons and positrons.

Fig. 9.4 A plasma crystal (from C.F. Driscoll et al., Physica C: Superconductivity **369**, Nos. 1–4, 21 (2002).) This is produced in a Penning trap such as the one in Fig. 9.2

9.3 Pair-ion Plasmas

One would expect that a plasma with equal masses would behave quite differently from a normal plasma with slow ions immersed in a sea of fast electrons. Though it is possible to make a positronium plasma, the recombination rate is so fast that there is no time to do experiments. Fullerenes, stable molecules of 60 carbon atoms arranged in a hollow sphere, move and recombine slowly because of the large mass. It is thus possible to produce a long-lived pair-ion plasma with C_{60}. In Fig. 9.5, neutral C_{60} is injected from an oven. A ring of fast electrons up to 150 eV driven through the C_{60} forms C_{60}^{+} ions by ionization and C_{60}^{-} ions by attachment. A magnetic field confines the electrons but allows the heavy ions to diffuse into the center to form a fullerene pair-ion plasma. The plasma then passes through a hole into a chamber for experimentation.

Consider a singly charged pair-ion plasma with a common mass M and temperature KT. The equations of motion for the ions of charge + or − are

$$Mn_0 \frac{dv_\pm}{dt} = \pm n_0 E - \nabla p. \tag{9.8}$$

Assuming waves of the form $\exp[i(kz - \omega t)]$ and $E = -\nabla\phi = -ik\phi$, we have

$$-i\omega M n_0 v_\pm = \mp ikn_0 e\phi - 3KTikn_\pm, \tag{9.9}$$

$$v_\pm = \frac{k}{\omega}\left(\pm\frac{e\phi}{M} + c_s^2\frac{n_\pm}{n_0}\right), \quad \text{where} \quad c_s^2 \equiv 3KT/M. \tag{9.10}$$

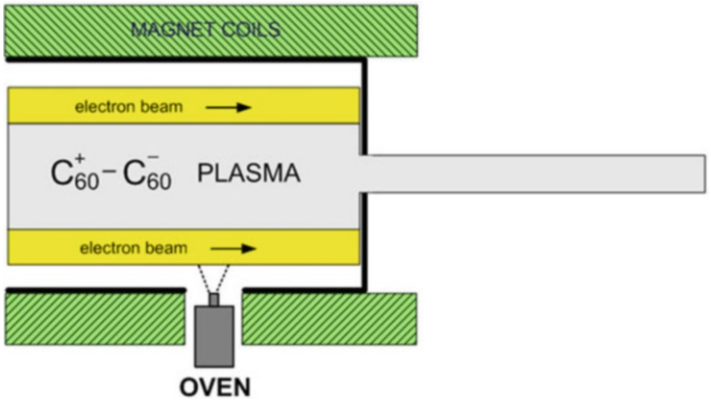

Fig. 9.5 Schematic of a fullerene plasma source. Adapted from W. Oohara and R. Hatakeyama, Phys. Plasmas **14**, 055704 (2007)

From the equation of continuity $\partial n/\partial t + \nabla \cdot (nv) = 0$, we have

$$-i\omega n_{\pm} + ikn_0 v_{\pm} = 0, \qquad \frac{n_{\pm}}{n_0} = \frac{k}{\omega} v_{\pm}. \tag{9.11}$$

Using this in Eq. (9.9), we find

$$\begin{aligned} -i\omega v_{\pm} &= \mp ik(e/M)\phi - ik(k/\omega)c_s^2 v_{\pm}, \\ v_{\pm}\left(1 - \frac{k^2}{\omega^2}c_s^2\right) &= \pm\frac{k}{\omega}\frac{e\phi}{M}. \end{aligned} \tag{9.12}$$

There are two solutions, depending on whether ϕ is zero. If ϕ is zero, the + and − ions move together without creating an E-field, and we have an ordinary sound wave:

$$\omega^2/k^2 = c_s^2. \tag{9.13}$$

If ϕ is not zero, Eq. (9.12) says that $v_+ = -v_-$. Then

$$\frac{n_{\pm}}{n_0} = \frac{k}{\omega} v_{\pm} = \pm k^2 \frac{e\phi/M}{\omega^2 - k^2 c_s^2}. \tag{9.14}$$

Poisson's equation then yields

$$\varepsilon_0 k^2 \phi = e(n_+ - n_-) = e n_0 k^2 \frac{2k^2 e\phi/M}{\omega^2 - k^2 c_s^2}$$

$$1 = \frac{en_0}{\varepsilon_0}\frac{2e/M}{\omega^2 - k^2c_s^2} = \frac{2\Omega_p^2}{\omega^2 - k^2c_s^2},$$
$$\omega^2 = k^2c_s^2 + 2\Omega_p^2 \tag{9.15}$$

where Ω_p is the ion plasma frequency $(ne^2/\varepsilon_0 M)^{1/2}$. Thus, a pair-ion plasma supports an ion acoustic wave and an ion plasma wave. The latter (Eq. (9.15)) is the analog of the Bohm-Gross wave of Eq. (4.30), but with a factor two because of the two ion species. These two waves are connected by an intermediate-frequency wave which can be derived only with kinetic theory.

9.4 Dusty Plasmas

In Chap. 5 we considered three-component plasmas consisting ions, electrons, and neutral atoms in partially ionized plasmas. In general, there can be contaminants of macroscopic size, "dust", made of other atomic species. In outer space, comet tails are dusty plasmas, as are some nebulas, such as the Orion nebula, and planetary rings, such as the one on Saturn. On earth, dusty plasmas can exist in flames; rocket exhausts; thermonuclear explosions; atmospheric-pressure plasmas (Sect. 9.6); and, importantly, in plasma processing (see Chap. 10). We shall find that dust has two main effects. First, it introduces low-frequency waves in the motions of the charged dust. Second, it changes the quasineutrality condition so that n_e is no longer equal to Zn_i, thus modifying the normal waves in the plasma.

Dust grains have sizes from tens of nanometers to hundreds of microns. Since electrons impinge on them much more often than ions do, the grains will have a negative surface potential V_s. Consider a spherical grain of radius a and charge $q < 0$. The capacitance of the sphere (with distant walls) is

$$C = 4\pi\varepsilon_0 a. \tag{9.16}$$

The surface charge q is then

$$q = CV_s = 4\pi\varepsilon_0 a V_s. \tag{9.17}$$

The value of either q or V_s depends on the Debye length λ_D in the background plasma.

If λ_D is $\ll a$, the grain is a small, isolated particle like a spherical Langmuir probe (Sect. 8.2.5). An ion will be attracted to the grain and will either strike it or orbit around it, depending on its orbital angular momentum around the grain. Enough electrons will be collected to ensure that the net current is zero. The required value of V_s is the "floating potential" of probe theory, which we need not discuss here. On the other hand, if λ_D is $\gg a$, the grains are a third charged component of the plasma along with the ions and electrons. For instance, in a Cs

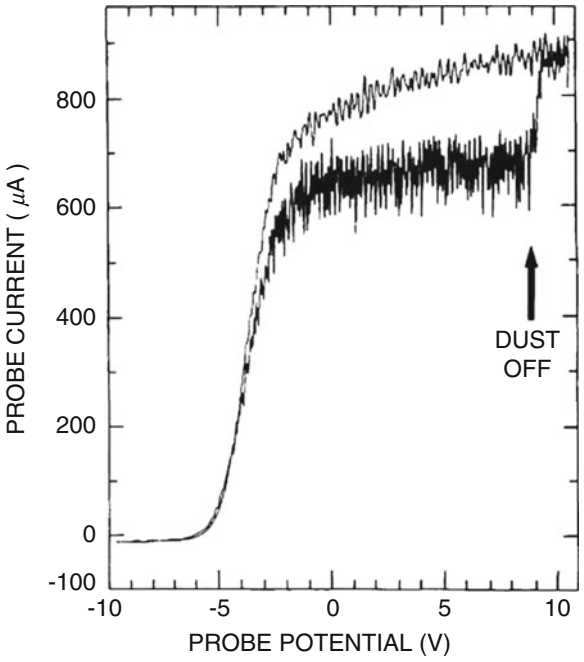

Fig. 9.6 Langmuir probe traces of a Q-machine plasma with (*bottom trace*) and without (*top trace*) dust. (A. Barkan, N. D'Angelo, and R. L. Merlino, Phys. Rev. Lett. **73**, 3093 (1994))

plasma with $KT = 0.21$ eV, λ_D is 34 μm at $n = 10^{10}$ cm^{-3} while $a \approx 1$ μm, so that $\lambda_D \gg a$ is satisfied.

Assume the latter condition, and let the dust grains have a charge $Z_d < 0$ and a density n_d. Charge neutrality requires

$$n_i = n_e - Z_d n_d. \tag{9.18}$$

Thus, the "electron" density is lowered by the presence of dust. This has been observed by Barkan et al. in a potassium Q-machine (Fig. 4.14). The dust, consisting of aluminum silicate particles of 5-μm average radius, was dropped into the plasma through a mesh on a rotating cylinder surrounding the plasma. The dust density was about 5×10^4 cm^{-3}. Figure 9.6 shows Langmuir probe traces of the plasma with and without the dust. In the presence of dust, the electron saturation current is seen to be lowered by the slow velocities of the heavy dust.

Studies of how dust is charged include many minor effects too detailed to be described here; for instance, secondary electron emission upon ion or electron impact, photoemission of electrons (often the dominant mechanism in cosmic plasmas), and field emission. It is not surprising that dust particles can arrange themselves in crystal arrays. Figure 9.7 shows how a picture of such a crystal can be obtained. A plasma is formed by RF applied to the bottom electrode, and dust is introduced by a shaker that is not shown; The dust is illuminated by a laser beam spread into a plane by a cylindrical lens, and a camera records the dust through a hole in the upper, grounded electrode. The dust is suspended above the RF

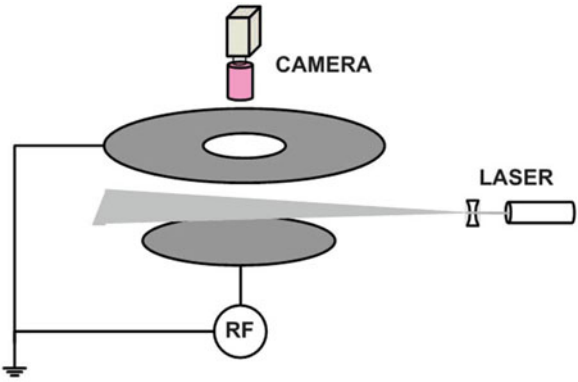

Fig. 9.7 Schematic of a setup to photograph the motion of dust grains in an RF plasma. The laser beam is spread into a sheet by a lens, shown rotated 90°. The dust dispenser is not shown. (Adapted from G. E. Morfill and H. Thomas, J. Vac. Sci. Technol. A **14**, 490 (1996))

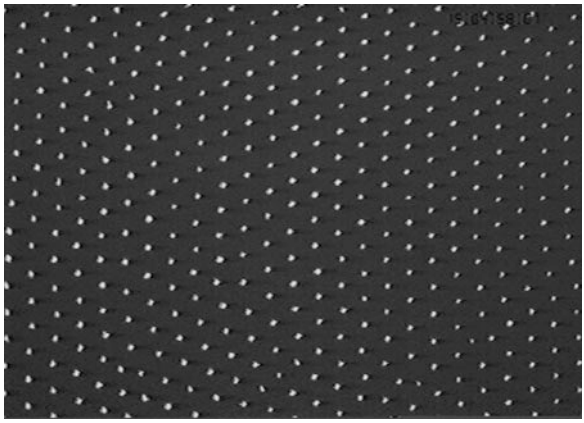

Fig. 9.8 Picture of a dust crystal taken by Morfill et al. (*loc. cit.*) with the apparatus shown in Fig. 9.7. The grains are trapped in the sheath on the lower electrode

electrode, which is negative relative to the plasma. A still picture of a dust crystal array is shown in Fig. 9.8.

By adding straight barriers to make a channel on the lower electrode, linear arrays of dust particles can be produced, as shown in Fig. 9.9. These can be pushed by the laser from the right. Only the first particle is pushed, and the others maintain the crystal spacing.

When the dust density is sufficiently high, the charged dust in a plasma can be considered as an additional fluid component exhibiting collective effects. The presence of charged dust in a plasma modifies all of the wave modes in Chap. 4, even with a DC magnetic field, and introduces new "dust waves" involving the motions of the charged dust. The dispersion relations for the plasma waves are modified through the quasi-neutrality condition (Eq. (9.18)), an example of which is the "dust ion-acoustic wave", which is analyzed below. We begin by considering the dust acoustic wave, which is a very low frequency, longitudinal, compressional wave involving the dynamics of the dust particles in a plasma.

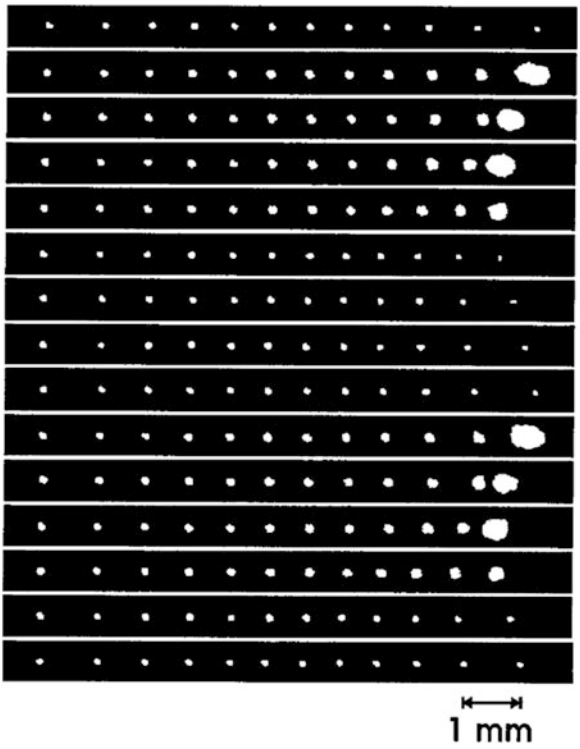

Fig. 9.9 A linear array of dust particles pushed by a laser from the right. The frames are 100 ms apart. (A. Homann et al., Phys. Rev. E **56**, 7138 (1997); P.K. Shukla and A. A. Mamun, *Intro. to Dusty Plasma Physics* (IOP Press, Bristol, UK, 2002.)

9.4.1 Dust Acoustic Waves

The dust acoustic wave is a very low-frequency, longitudinal compressional wave involving the motions of the dust particles. Because the heavy dust moves more slowly than the ions and electrons, the latter have time to relax into Maxwellian distributions:

$$\begin{aligned} n_e &= n_{e0}\exp(e\phi/KT_e) = n_{e0}(1 + e\phi/KT_e + \ldots), \quad n_{e1} = n_{e0}(e\phi/KT_e) \\ n_i &= n_{i0}\exp(-e\phi/KT_i) = n_{i0}(1 - e\phi/KT_i + \ldots), \quad n_{i1} = n_{i0}(-e\phi/KT_i) \end{aligned} \tag{9.19}$$

Using the subscript d for dust, we can write the 1-D dust equations of motion and continuity as:

$$\frac{\partial \mathbf{v}_d}{\partial t} = -\frac{q_d}{M_d}\nabla\phi - v_{thd}^2\frac{\nabla n_{d1}}{n_{d0}} \tag{9.20}$$

$$\frac{\partial n_{d1}}{\partial t} + n_{d0}\nabla \cdot \mathbf{v}_d = 0, \tag{9.21}$$

$$\text{where} \quad v_{thd}^2 \equiv 3KT_d/M_d, \tag{9.22}$$

and the subscript *1* has been dropped from v_{d1} since $v_{\mathrm{d0}} = 0$. Poisson's equation is

$$\nabla^2\phi = \frac{1}{\varepsilon_0}(en_{e1} - en_{i1} - q_d n_{d1}). \tag{9.23}$$

The dust charge is taken to be constant. To express n_{d1} in terms of ϕ, take the time derivative of Eq. (9.21) and use Eq. (9.20):

$$\begin{aligned}\frac{\partial^2 n_{d1}}{\partial t^2} &= -n_{d0}\nabla \cdot \frac{\partial v_d}{\partial t} = -n_{d0}\nabla \cdot \left(-\frac{q_d}{M_d}\nabla\phi - v_{thd}^2\frac{\nabla n_{d1}}{n_{d0}}\right) \\ &= n_{d0}\frac{q_d}{M_d}\nabla^2\phi + v_{thd}^2\nabla^2 n_{d1} \\ \text{or} \quad &\left(\frac{\partial^2}{\partial t^2} - v_{thd}^2\nabla^2\right)n_{d1} = \frac{q_d n_{d0}}{M_d}\nabla^2\phi.\end{aligned} \tag{9.24}$$

Using Eq. (9.19) in Eq. (9.23) gives

$$\nabla^2\phi = \left(\frac{n_{e0}e^2}{\varepsilon_0 KT_e} + \frac{n_{i0}e^2}{\varepsilon_0 KT_i}\right)\phi - \frac{eZ_d}{\varepsilon_0}n_{d1} = \left(k_{De}^2 + k_{Di}^2\right)\phi - \frac{eZ_d}{\varepsilon_0}n_{d1}, \tag{9.25}$$

where $k_{Dj}^2 \equiv n_{j0}e^2/\varepsilon_0 KT_j$, so that, with $k_D^2 \equiv k_{De}^2 + k_{Di}^2$, Eq. (9.25) simplifies to

$$\nabla^2\phi = k_D^2\phi - (eZ_d/\varepsilon_0)n_{d1} \tag{9.26}$$

Remembering that n_{d1} is the density fluctuation of a dust wave, we can let n_{d1} and ϕ take the usual form $\exp[i(kz - \omega t)]$. Equations (9.24) and (9.26) then become, respectively,

$$\left(\omega^2 - k^2 v_{thd}^2\right)n_{d1} = \frac{eZ_d n_{d0}}{M_d}k^2\phi \tag{9.27}$$

and

$$\left(k^2 + k_D^2\right)\phi = \frac{eZ_d}{\varepsilon_0}n_{d1}. \tag{9.28}$$

Thus,

$$k^2 + k_D^2 = \frac{n_{d0}e^2Z_d^2}{\varepsilon_0 M_d}\frac{k^2}{\left(\omega^2 - k^2 v_{thd}^2\right)}. \tag{9.29}$$

The coefficient on the r.h.s can be called the square of the "dust plasma frequency" ω_{pd} in analogy with Eq. (4.25). The dispersion relation for these low-frequency *dust acoustic waves* is then

$$1+\frac{k_D^2}{k^2}-\frac{\omega_{pd}^2}{\omega^2-k^2v_{thd}^2}=0,\quad \omega_{pd}\equiv\left(\frac{n_{d0}e^2Z_d^2}{\varepsilon_0 M_d}\right)^{1/2}, \tag{9.30}$$

where k_D refers to the electron-ion plasma. In laboratory plasmas, typically $KT_\mathrm{e}\gg KT_\mathrm{i}$, so that $k_D^2\approx k_{Di}^2=\lambda_{Di}^{-2}=n_{i0}e^2/\varepsilon_0 KT_i$ and

$$\omega^2-k^2v_{thd}^2=\frac{k^2\omega_{pd}^2}{k^2+k_{Di}^2}=\frac{k^2\lambda_{Di}^2\omega_{pd}^2}{1+k^2\lambda_{Di}^2}. \tag{9.31}$$

We can define

$$c_d\equiv\omega_{pd}\lambda_{Di}=\left(\frac{n_{d0}}{n_{i0}}Z_d^2\frac{KT_i}{M_d}\right)^{1/2} \tag{9.32}$$

as the dust acoustic speed, in analogy with $c_s=\omega_p\lambda_D$. For cold dust, we can neglect v_thd, and then have for the phase velocity

$$\frac{\omega}{k}\approx\frac{c_d}{\left(1+k^2\lambda_{Di}^2\right)^{1/2}}. \tag{9.33}$$

For $k^2\lambda_{Di}^2<<1$, the waves are non-dispersive sound-like waves with $\omega/k\approx c_d$. These dust plasma waves, with $c_d\propto 1/M_d^{1/2}$, propagate very slowly. For example, in a typical laboratory dusty plasma with dust particles of 1 μm size, $KT_\mathrm{e}=2.5$ eV, $KT_\mathrm{i}=0.025$ eV, $Z_\mathrm{d}\approx 2000$, $M_d\approx 10^{-15}$ kg, and $n_{d0}/n_{i0}\sim 10^{-5}$, the dust acoustic speed c_d is ~1 cm/s. Dust acoustic waves can be seen by illuminating the dust with a thin sheet of laser light as shown in Fig. 9.7. Figure 9.10 shows a frame from a video of a dust acoustic wave.

9.4.2 *Dust Ion-acoustic Waves*

Dust has a physically reasonable effect on the normal ion waves of Sect. 4.6. The ion equations of motion and continuity are:

$$\frac{\partial\mathbf{v}_i}{\partial t}=-\frac{e}{M}\nabla\phi-\mathbf{v}_{thi}^2\frac{\nabla n_{i1}}{n_{i0}} \tag{9.34}$$

$$\frac{\partial n_{i1}}{\partial t}+n_{i0}\nabla\cdot\mathbf{v}_i=0. \tag{9.35}$$

Inserting Eq. (9.34) into the time derivative of Eq. (9.35) gives

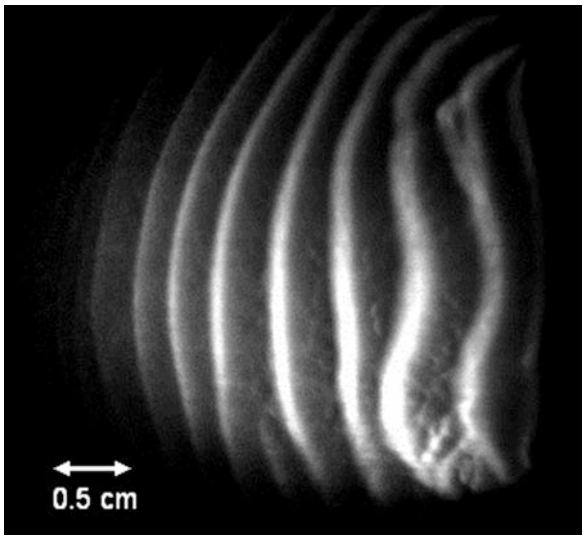

Fig. 9.10 A single-frame video image of a dust acoustic wave propagating from *right* to *left*. The bright vertical features are the wave crests imaged from scattered laser light (courtesy of R. Merlino)

$$\left(\frac{\partial^2}{\partial t^2} - v_{thi}^2 \nabla^2\right) n_{i1} = n_{i0} \frac{e}{M} \nabla^2 \phi. \tag{9.36}$$

Again let the waves have the usual form $\exp[i(kz - \omega t)]$, so that

$$\left(\omega^2 - k^2 v_{thi}^2\right) n_{i1} = \frac{e n_{i0}}{M} k^2 \phi. \tag{9.37}$$

Since the phase velocity ω/k will be scaled to KT_e, as in ion sound waves, and $KT_i \ll KT_e$, the ${v_{thi}}^2$ term can be neglected, so that

$$\omega^2 n_{i1} = \frac{e n_{i0}}{M} k^2 \phi, \text{ and, similarly, } \omega^2 n_{d1} = \frac{q_d n_{d0}}{M_d} k^2 \phi. \tag{9.38}$$

Using Eq. (9.19) for n_{e1} and Eq. (9.38) for n_{i1} and n_{d1} in Eq. (9.23) yields

$$\begin{aligned} -k^2 \phi &= \left(k_{De}^2 \phi - \frac{k^2}{\omega^2} \omega_{pi}^2 \phi - \frac{k^2}{\omega^2} \omega_{pd}^2 \phi\right), \\ 1 + \frac{k_{De}^2}{k^2} &= \frac{\omega_{pi}^2}{\omega^2} + \frac{\omega_{pd}^2}{\omega^2} \end{aligned} \tag{9.39}$$

The phase velocity is then given by

$$\frac{\omega^2}{k^2} = \frac{\omega_{pi}^2 + \omega_{pd}^2}{k^2 + k_{De}^2} \approx \frac{\omega_{pi}^2 \lambda_{De}^2}{1 + k^2 \lambda_{De}^2}. \tag{9.40}$$

Since $Z_d n_{d0}$ is at most n_{i0}, the ratio ${\omega_{pd}}^2/{\omega_{pi}}^2 = (n_{d0}/n_{i0})({Z_d}^2 M/M_d)$ is less than $Z_d M/M_d$. We can then neglect the ${\omega_{pd}}^2$ term and have done so. Equation (9.40) justifies the definition of c_d as a phase velocity in Eq. (9.32).

If n_{0e} is not so small that λ_D is as large as the wavelength of the wave, we can neglect the $k^2\lambda_{De}{}^2$ term in the denominator of Eq. (9.40). Also, q_d is usually much larger than e, so n_e can be much smaller than n_i. The numerator is then

$$\omega_{pi}^2\lambda_{De}^2 = \frac{n_{0i}e^2}{\varepsilon_0 M}\frac{\varepsilon_0 KT_e}{n_{0e}e^2} = \frac{n_{0i}}{n_{0e}}c_s^2 >> c_s^2.$$

Equation (9.40), finally, gives the phase velocity

$$\frac{\omega}{k} = \left(\frac{n_{0i}}{n_{0e}}\right)^{1/2} c_s. \tag{9.41}$$

This is the dispersion relation for dust-modified ion acoustic waves, or dust ion acoustic waves. The dust density does not appear explicitly here, but it determines the n_{i0}/n_{e0} ratio via the quasineutrality condition $n_{i0} = n_{e0} + |Z_d|n_{d0}$ (Eq. (9.18)) for negatively charged dust. In terms of the dust fraction $\delta \equiv n_{d0}/n_{i0}$, we can write Eq. (9.41) as

$$\frac{\omega^2}{k^2} = \left(\frac{n_{i0}}{n_{i0} - |Z_d|n_{d0}}\right)c_s^2 = \frac{c_s^2}{1 - \delta|Z_d|}.$$

Thus, the phase velocity is

$$\frac{\omega}{k} = \frac{c_s}{\left(1 - \delta|Z_d|\right)^{1/2}}, \qquad \delta = n_{d0}/n_{i0}. \tag{9.42}$$

This shows that dust increases the velocity of ion acoustic waves, with the consequence that Landau damping of those waves is decreased.

9.5 Helicon Plasmas

So far, we have mainly treated plasmas consisting of charged species: negative ones, such as electrons and charged dust; and positive ones, such as ions and positrons. Such fully ionized plasmas, however, have to be specially prepared in the laboratory in fusion devices, Q-machines, and such. Most laboratory plasmas are partially ionized and include neutral atoms. Collisions with neutrals were considered in Chap. 5 on diffusion. Plasmas that have practical applications, such as semiconductor etching and magnetic sputtering, are partially ionized. The granddaddy of three-component plasmas is the helicon plasma, which includes not only neutrals but also a magnetic field. Though helicons are complicated, they have been studied exhaustibly worldwide and are well understood.

Helicon plasmas are ionized by helicon waves, which are basically whistler waves (R waves) confined to a cylinder. Their frequencies generally lie between ω_c and the lower hybrid frequency ω_l (Eq. (4.71)). To satisfy the boundary conditions on the cylinder, a second wave has to be generated near the boundary. This second wave is an electron cyclotron wave traveling obliquely to the B-field; it is called the Trivelpiece-Gould (TG) mode (Fig. 4.21). Let β be the total k such that $\beta^2 = k_\perp^2 + k_z^2$. The R wave dispersion relation for propagation at an angle θ to **B** is (Problem 9.2)

$$\frac{c^2\beta^2}{\omega^2} = 1 - \frac{\omega_p^2/\omega^2}{1-(\omega_c/\omega)\cos\theta} \underset{\omega_c >> \omega}{\longrightarrow} \frac{\omega_p^2}{\omega\omega_c\cos\theta}. \tag{9.45}$$

Defining $k \equiv k_z = \beta\cos\theta$, we have

$$\beta = \frac{\omega^2}{c^2}\frac{1}{\beta}\frac{\omega_p^2}{\omega\omega_c\cos\theta} = \frac{\omega}{c^2}\frac{\omega_p^2}{\omega_c}\frac{1}{k} = \frac{\omega}{k}\varepsilon_0\mu_0\frac{n_0e^2}{\varepsilon_0 m}\frac{m}{eB_0}$$

Thus,

$$\beta = \frac{\omega}{k}\frac{n_0 e\mu_0}{B_0}. \tag{9.46}$$

This is the basic equation for helicon waves. It shows that the density increases linearly with B_0, and the electron mass m has cancelled out to this order. The frequency is much lower than the electron frequencies ω_c and ω_p. When terms in m are kept, a second wave, the TG mode, is obtained. The relation between the helicon (H) and TG waves has been clarified in papers by D. Arnush, who also wrote a computer program HELIC for the properties of these waves. Damping by electron-neutral collisions is important in the exact theory. The relation between the H and TG waves is shown in Fig. 9.11. There, k (the wave number parallel to B_0) is plotted against β, the cylindrical wave number in the radial direction, for azimuthal wave number $m = 1$. Above a minimum, there are two solutions for k for given n and B_0, the one with large β being the TG mode.

Helicon discharges have been studied experimentally in many machines with long, uniform magnetic fields of order 0.1 T. The first such machine, built by R.W. Boswell in Australia, reached a density of almost 10^{20} m^{-3} on axis. Different types of antennas have been used, the most efficient being helical ones matching the helicity of $m = +1$ waves obeying Eq. (9.46). For reasons not well understood, $m = -1$ waves rotating in the opposite direction do not propagate as well. The coupling of radiofrequency (RF) energy from the antenna to the plasma has been found to involve parametric instabilities. Instabilities such as the drift-wave instability (Fig. 6.14) have been studied in helicon discharges. Magnetic confinement of electrons (but not of argon ions, which have Larmor orbits larger than the discharge radius), combined with efficient antenna coupling, enables helicons to achieve

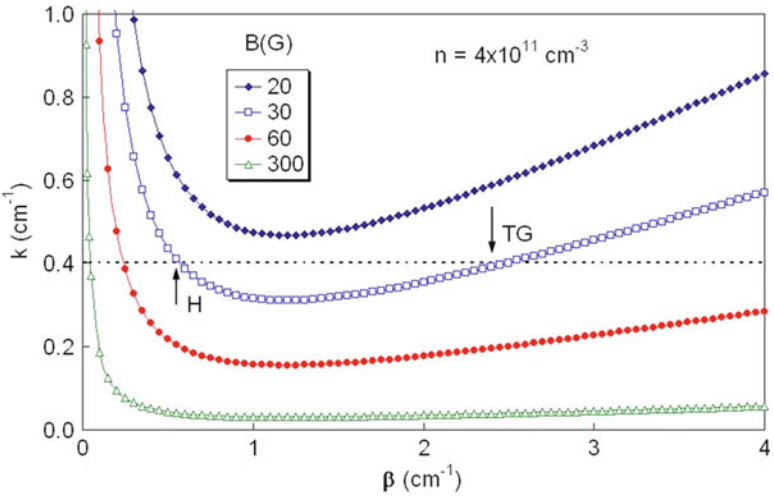

Fig. 9.11 The dispersion relation for $m = 1$ helicon and TG waves at one density and four magnetic fields (F.F. Chen, Plasma Sources Sci. Technol. **24**, 014001 (2015))

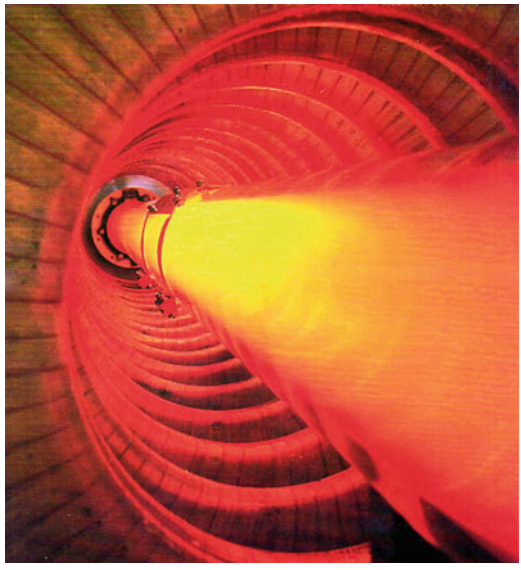

Fig. 9.12 A large helicon discharge inside its magnet coils (R.T.S. Chen, R.A. Breun, S. Gross, N. Hershkowitz, M.J. Hsieh, and J. Jacobs, Plasma Sources Sci. Technol. **4**, 337 (1995))

higher densities than in other RF plasmas at the same power. However, the expense of a DC B-field has so far prevented helicons from being accepted by industry. To overcome this, arrays of short helicon discharges with permanent magnets have been proposed for producing large, uniform, high-density plasmas for plasma processing (see Sect. 10.3).

Figure 9.12 shows a large helicon discharge. Note that At high B-field and high power, the plasma can shrink into a dense blue core which is almost fully ionized.

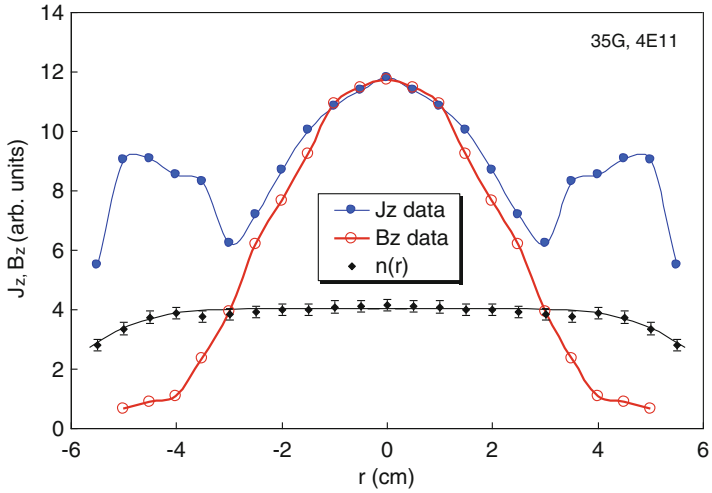

Fig. 9.13 Radial profiles of $n(r)$, $B_z(r)$, and $J_z(r)$ in a helicon discharge at $B = 3.5$ mT and $n = 4 \times 10^{17}$ m^{-3} (D.D. Blackwell, T.G. Madziwa, D. Arnush, and F.F. Chen, Phys. Rev. Lett. **88**, 145002 (2002))

Helicon devices proposed for semiconductor etching and spacecraft propulsion will be shown in Chap. 10.

The phase velocity of helicon waves along **B** is usually comparable to the velocities of "primary" electrons... those that do the ionization. This fact gave rise to a hypothesis that helicons accelerate the ionizing electrons by inverse Landau damping. However, measurements of electron velocity distributions showed no such population of fast electrons. It turns out that most of the RF energy goes into the TG mode near the radial boundary, where the antenna is; and only a small amount goes directly into the helicon mode, which peaks near the axis. The TG wave then couples to helicon waves to form a combined TG-helicon wave. The TG wave parametrically decays into electron cyclotron waves, as mentioned above, and the latter heats the electrons by collisional damping. Though the TG wave is an essential part of the RF coupling, it is not easily detected because it is normally localized to a thin layer near the surface. By lowering the B-field to thicken the layer, and measuring the RF current rather than the RF B-field, the TG wave can be detected, as shown in Fig. 9.13. The current profile shows large peaks due to the TG mode, but these are not seen in the B-field profile.

9.6 Plasmas in Space

As we leave the earth, we first encounter plasmas in the ionosphere, where auroras are born about 100 km above the earth. Further out are the Van Allen radiation belts, filled with plasma from the solar wind. Further yet is the magnetosphere

where the B-fields of the sun and the earth collide, and, on the night side, the magnetotail, where reconnection takes place (Fig. 8.31). The sun has important plasma effects in its prominences, flares, and sunspots. The outer planets have plasma in their atmospheres and rings. Space plasma physics is the study of these plasmas in the solar system. Plasma astrophysics, on the other hand, concerns plasmas in the rest of the universe. Galaxies contain plasmas in stars, gas clouds, and black holes. Pulsars, quasars, and active galactic nuclei are all astrophysical plasmas, some with extreme properties. Neutron stars, for instance, have densities of order 4×10^{17} kg/m^3. A sugar-cube sized piece (1 cm^3) of this material would weigh as much as 1.3 million Eiffel towers.

Auroras are produced by ions and electrons of energies of about 100–1000 eV which reach down to altitudes of about 100 km. They excite the oxygen and nitrogen atoms in the atmosphere, giving off green and brown light from oxygen and blue and purple light from nitrogen. Striking displays of Aurora Borealis are observed in northern latitudes. Aurora Australis also occurs in Antarctica but is seen mostly by penguins. In outer space all that we can see must be in the plasma state, but this is only a tiny fraction of a universe containing dark energy, dark matter, and black holes. Nonetheless, astrophysics cannot be studied without the language of plasma physics.

9.7 Atmospheric-Pressure Plasmas

When a voltage is applied between two electrodes in air, a spark will form between the electrodes, forming a plasma, when the voltage is high enough. This breakdown, studied in 1889 by F. Paschen, was perhaps the first plasma experiment. The breakdown voltage depends on the gas, the pressure p, and the distance d between the electrodes. Figure 9.14 shows this relationship in a modern experiment in argon, where contaminants such as moisture are absent. When pd is small, electrons' mean free paths are longer than d, and large voltages are required to accelerate ions to energies that can release secondary electrons from the surface. When pd is large, electrons lose energy in collisions with the neutral gas, and the voltage rises again. Thus there is a minimum in the Paschen curve. After breakdown between parallel plates, the current is not uniform but tends to flow in streamers, each reaching its own equilibrium.

In such an equilibrium, each time an ion strikes the negative plate (the cathode), γ electrons are released, γ being the secondary electron emission coefficient. These electrons are accelerated by the sheath into the plasma and collide with neutrals to form new electron-ion pairs. Each new ion will strike the cathode to release more secondary electrons, thus creating an avalanche. The density will exponentiate. Let α be the probability for an ionizing collision in a unit distance. Clearly α is proportional to $1/\lambda_{\text{mfp}}$, where λ_{mfp} is the mean free path for ionization. One electron will generate $e^{\alpha d}$ ion-electron pairs in a distance d. Upon colliding with the cathode,

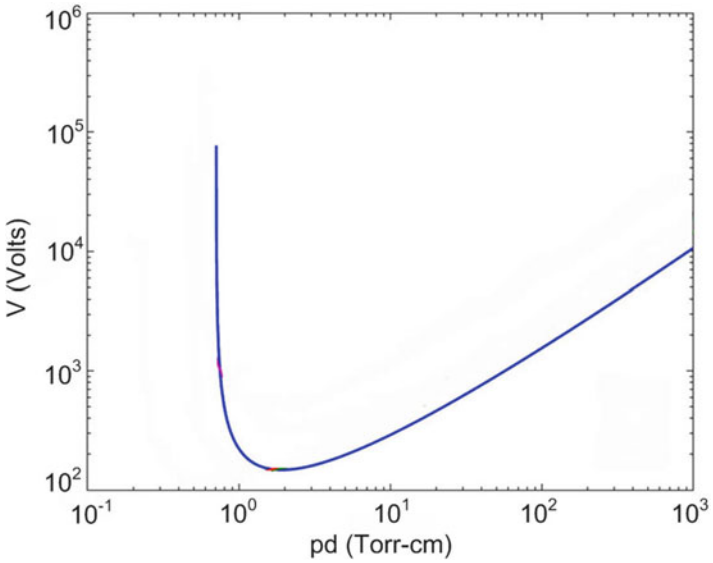

Fig. 9.14 A Paschen curve for argon

these ions will generate $\gamma(e^{\alpha d} - 1)$ new electrons. In equilibrium this has to reproduce exactly the original electron. Thus steady state requires

$$\gamma\left(e^{\alpha d} - 1\right) = 1. \tag{9.47}$$

This is called a *Townsend discharge*. The symbols α and γ are also used to denote two regimes of RF discharges, a low-current and a high-current regime, with a discontinuous jump between the two.

9.7.1 Dielectric Barrier Discharges

To prevent sparking at atmospheric pressures, a dielectric barrier can be inserted between the two electrodes. In Fig. 9.15, the electrodes are covered with insulating dielectric, and high-voltage pulses create the plasma by capacitive coupling. In Fig. 9.16, a dielectric barrier separates the electrodes, but the E-field extends into the space above to ionize the plasma. The substrate to be treated is passed horizontally through the plasma.

Dielectric barrier discharges are used in xenon lamps and for the pixels in plasma display panels (TV screens), for instance.

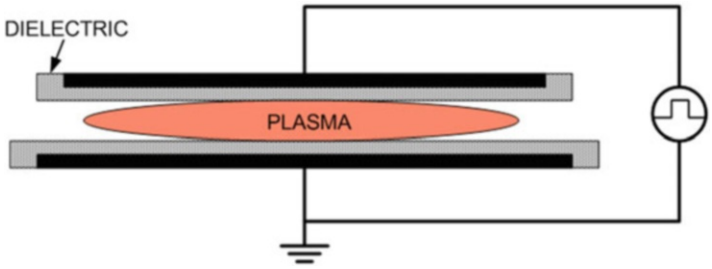

Fig. 9.15 A dielectric barrier discharge of Type 1

Fig. 9.16 A dielectric barrier discharge of Type 2

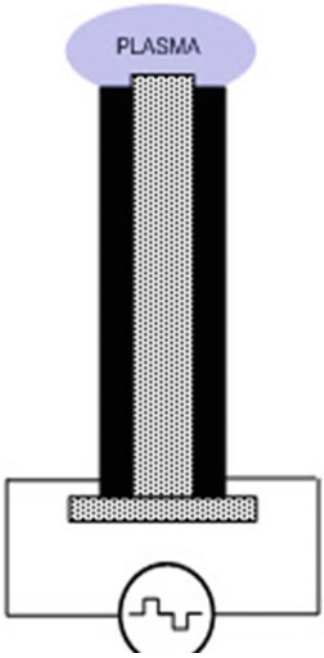

9.7.2 RF Pencil Discharges

Another type of discharge that operates at atmospheric pressure is in the shape of a pencil, as shown in Fig. 9.17. The plasma is excited with RF or microwaves to prevent arcing. In one commercial application, a mixture of helium and oxygen is injected, and 200 W of RF at the industrial frequency of 13.56 MHz is applied between the center tube and ground. A plasma beam about two inches long is formed with density up to 10^{13} cm^{-3}, compared to normal air density of 3×10^{19} cm^{-3}. Since no vacuum system is required, these beams can be used medically for cauterizing skin and for some dental procedures. The beam can also

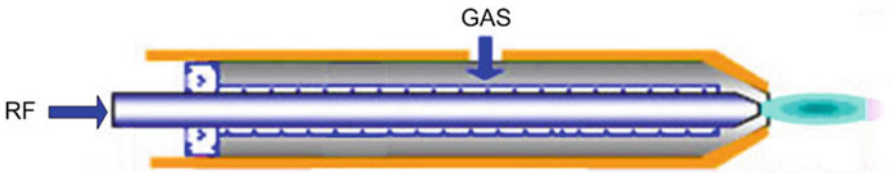

Fig. 9.17 Schematic of a pencil-type atmospheric plasma

be scanned, line by line, over a large surface that requires plasma treatment, such as cleaning or deposition. To treat a wire-shaped object, an atmospheric plasma can be made inside a cylinder through which the wire is passed. Conversely, a catheter can be sterilized with a plasma created with a wire inside it.

A duodenoscope is a small medical instrument inserted into the small intestine to treat such conditions of the bile ducts and main pancreatic duct. These devises have very small openings which are difficult to sterilize. In 2015, numerous deaths were caused by a superbug known by the acronym CRE which survives normal sterilization methods. Since bacteria would be killed by a plasma at 1 or 2 eV, duodenoscopes could be cleaned with an atmospheric plasma, since the small mean free path of electrons in air would allow them to enter very small cavities. In recent years atmospheric pencil plasmas have become widely used in the medical profession.

Problems

9.1 A C_{60} pair-ion plasma is created with a temperature $KT = 0.3$ eV. Describe the sheath at the end walls that intercept the magnetic field lines.

9.2 Modify the R- and L-wave dispersion relations for propagation at an angle θ to $\mathbf{B}$.